Dislocation nucleation induced by a shock wave in a perfect crystal: Molecular dynamics simulations and elastic calculations

D. Tanguy,[1,2,*] M. Mareschal,[1] P. S. Lomdahl,[3] T. C. Germann,[3] B. L. Holian,[3] and R. Ravelo[4]
[1]*Centre Européen de Calcul Atomique et Moléculaire, Ecole Normale Supérieure, 46, Allée d'Italie, Fr-69007 Lyon, France*
[2]*CNRS, URA 1884, Ecole des Mines de Saint-Etienne, 158 cours Fauriel, Fr-42023 Saint-Etienne, France*
[3]*Theoretical Division, Los Alamos National Laboratory, Los Alamos, New Mexico 87545, USA*
[4]*Department of Physics, University of Texas, El Paso, Texas 79968-0515, USA*
(Received 7 March 2003; published 27 October 2003)

We study the nucleation mechanism of the defects responsible for plastic flow in a ⟨100⟩ fcc perfect single crystal submitted to a shock wave. In the large-scale nonequilibrium molecular dynamics simulation, small dislocation loops are created from thermal fluctuations just behind the shock front, in a narrow region of a few lattice parameters width. Their critical size is measured. The activation energy for the formation of an edge dipole, under high pressure, is computed within the Peierls framework. The elastic constants and the generalized stacking fault energy are computed from the interatomic potential. This model enables a qualitative discussion of the influence of material parameters such as intrinsic and unstable stacking faults versus elastic energy release.

DOI: 10.1103/PhysRevB.68.144111 PACS number(s): 62.20.Fe, 62.50.+p, 02.70.Ns

I. INTRODUCTION

The propagation of a shock wave involves the displacement of an interface between the initial material (cold and relaxed) and the highly compressed final state. Above a certain shock strength, the unaixially compressed material is unstable and relaxes to a hydrostatically compressed state, in general, by a plasticity mechanism. This occurs under a stress one or two orders of magnitude higher than the engineering yield stress (the deformation is of the order of 10%) and under extreme strain rates corresponding to shock velocities of the order of km/s, i.e., nm/ps. Smith[1] proposed a mechanism where yielding occurs in a narrow region behind the shock front by way of a two-dimensional (2D) array of dislocations. This array follows the front annihilating the lattice mismatch between the initial state and the hydrostatically compressed final state.

Recently, atomic scale simulations have addressed this problem in defect free single crystals (for a review, see Ref. 2). Nonequilibrium molecular dynamics (NEMD) using empirical interatomic potentials is well adapted because it gives the dynamics on a time scale compatible with the extreme strain rate. Previous work[3] has shown that in the ⟨100⟩ direction, the shear stress is released by the formation of a 3D mesostructure involving slippage along ⟨111⟩ planes. A fascinating, but still not fully understood, variety of plastic behavior has been found in the ⟨110⟩ and ⟨111⟩ directions.[4] It reveals the complexity of the crystal response, even in the case where no initial defects are present.

In this work, we study the nucleation of crystalline defects at the shock front, or at its immediate rear, in fcc ⟨100⟩ perfect single crystals. From earlier work,[4] it seems to be the simplest deformation mechanism, giving MD simulations the opportunity to reach an atomic description of the transition between the elastic wave of the first moments of propagation and the steady plastic wave. In the first part, we perform large-scale NEMD simulations of shock propagation above the elastic limit. Several criteria are developed to select the atoms which belong to the region of localized slip, therefore enabling a detailed study of the structure of the defects. The second part is dedicated to the measure of the relevant parameters for the nucleation: critical defect size, temperature, nucleation rate, propagation velocity. The third part focuses on the potential-energy barrier for nucleation. The Peierls model is combined with finite elements to deal with the specifics of high-pressure plasticity. This semiquantitative model separates the elastic contribution to the energy barrier from the nonlinear excess energy related to the displacement discontinuity across the slip plane. It is used to analyze the driving forces for the nucleation and propagation of plasticity at high pressure in terms of a limited number of parameters: the resolved shear deformation, the intrinsic stacking fault, and the unstable stacking fault at different uniaxial compressions.

II. DIRECT MD SIMULATION OF SHOCK-INDUCED PLASTICITY

A. Technique

We used NEMD computer simulations[5] to study a ⟨100⟩ fcc single crystal composed of $54\times54\times100$ unit cells (1.2×10^6 particles). The influence of the cross-sectional dimensions on plasticity has been evaluated in a previous work using box sizes up to 100×100 fcc unit cells.[3] We have checked that the results we obtain are in agreement with those obtained on bigger systems. The choice of a smaller system was made here because we are interested in the structure of lattice defects in the first stages of plasticity and not in the stationary shock structure. A limited number of particles, even if it involves more noise in the shock wave profiles, is easier to handle. This work will show that the size of the system is large enough to limit the influence of the boundaries on the nucleation of plasticity.

Periodic boundary conditions are applied in the x and y directions. Boundaries are free in the z direction, except that

a shock wave is created by giving the same velocity $-u_p$ to all atoms and imposing a momentum mirror at $z=0$. The initial temperature is given to the crystal by superimposing a random thermal velocity on every particle according to a Maxwell distribution. The particles interact via a Lennard-Jones (LJ) 6-12 pair potential. The range of the interactions is $2.3r_0$ (second and third neighbors contribute about 10% of the cohesive energy E_c each, while fourth and fifth have negligible contribution to E_c). The units are ϵ (bond energy), r_0 (bond distance), and m (the mass of the particle), from which the unit of time $t_0=r_0\sqrt{m/\epsilon}$ is determined. The main quantities measured during the simulation are the pressure in the z direction P_{zz}, the shear stress $(\tau=\frac{1}{2}[P_{zz}-\frac{1}{2}(P_{xx}+P_{yy})])$, the density profile ρ, and the transverse temperature (kT_t). This temperature is the mean kinetic energy in the transverse direction $[\frac{1}{2}(v_x^2+v_y^2)]$. It is an indicator of the transformation of the uniaxial kinetic energy $(\frac{1}{2}mu_p^2)$ into thermal kinetic energy. The local compression (relevant for the characterization of the onset of plasticity) is difficult to measure because the density fluctuations are high behind the shock front. Nevertheless, the average compression can be determined from the mass flux balance in a steady, planar (one-dimensional) shock: $\rho_0 u_s=\rho(u_s-u_p)$, where ρ_0 is the initial density of unshocked material, ρ is the final (shocked) density, u_p is the piston, or particle velocity behind the shock front, which propagates at velocity u_s. For a shock in the fcc $\langle 100\rangle$ direction, with a short-range LJ potential, Germann *et al.*[4] have measured an elastic limit of $0.2c_l$ which corresponds to a compression of 14%, the typical deformation we deal with in this paper.

B. Defect detection

One method widely used for the detection of dislocations in atomic scale simulations in fcc materials is the identification of local hcp configurations. These stacking faults are the traces left by the movement of Shockley partial dislocations. The method is based on the ''common neighbor analysis''[6] which can distinguish these structures by the difference in bonding between the common first neighbors of a pair of atoms.

Another method which provides quantitative information about the dislocation structure and position is proposed in Ref. 7. The measure of the slip distribution along the glide plane gives the Burgers vector *b*. Moreover, its gradient exhibits a peak at the position of the dislocation line, enabling a precise localization of the defect. This method can be used to characterize a slip defect when its nature is not precisely known, but, unfortunately, it requires too much work to be done ''on the fly,'' if one has no idea, *a priori*, on which plane slip will occur.

If we consider an ideal edge dislocation, at zero external stress, constructed by including an excess half plane on one side of the glide plane, its displacement will involve the propagation of a long-range displacement field of value *b*, even far away in the direction normal to the glide plane. In the case of plasticity induced by a shock wave in a perfect crystal, the nucleation and propagation of such dislocations should be done without incompatibility between their displacement fields. It is therefore quite intriguing to check how the defects rearrange in the steady state to avoid such incompatibilities. Therefore, the first criterion that we used detects the ''blocs'' of matter which are translated. To decrease the thermal noise, the positions are averaged over a few vibrational periods ($100\Delta t$, where $\Delta t=0.001t_0$ is the NEMD time step). Every atom with a transverse displacement higher than a threshold is preselected. Then, its first neighbors are tested. If more than one-half of its first neighbors are displaced by roughly the same amount, the atom is considered as belonging to a sheared bloc of matter and printed to the screen. The result is a map of the areas of homogeneous shear displacement (the compression in the *z* direction does not influence the criterion) which should highlight dislocation emission in the first moments of plasticity.

This criterion is designed to check for displacement incompatibilities; it does not provide ''clean'' pictures of the dislocation line. It can also lead to very high numbers of atoms selected in the case of high dislocation densities. Therefore, a complementary criterion is needed. We modified the ''centrosymmetry parameter'' developed by Kelchner,[8] which we call the ''modified centrosymmetry parameter'' (MCP). Its value at the atomic site i is

$$C_i=\sum_j \|\vec{r}_j+\vec{r}_{j+6}\|^2, \tag{1}$$

where $\vec{r}_j$ and $\vec{r}_{j+6}$ are the positions at time t of the first neighbors of atom i at time t_0, which at $t=0$ formed opposite pairs $(\vec{r}_j=-\vec{r}_{j+6})$. In our simulation, the crystal is perfect at time t_0, but the parameter can be used if the box contains initial defects, too. This criterion allows us to track the nucleation and propagation of any type of defect (point defects, dislocations). For example, after the passage of a perfect dislocation, the crystal shows no trace except that the neighbors of the atoms of the $\{111\}$ planes above and below the glide plane are no longer the same as before. They will have high MCP values. Therefore, the modified centrosymmetry parameter allows us to follow the ''trajectory'' of the defects, without knowing their nature *a priori*.

In brief, we have used criteria specific to large elastic compressions, which require no prior knowledge of the defect structure and are computationally very simple, for an efficient implementation in large-scale NEMD simulations.

C. Structural model

We performed NEMD simulations at piston velocities just above the elastic limit: $u_p=1.7$ and 1.9 in reduced LJ units $(\sqrt{\epsilon/m})$. At these velocities, the density of defects is low enough to enable a detailed study of the first few moments of their creation.

At the scale of the whole sample, plasticity can be detected by following the time evolution of the shear stress profile. Figure 1 shows three profiles at different times. The shock wave propagates from the left to the right in the longitudinal direction *z*. As previously reported,[3] shock propagation is elastic during a relaxation time before the shear stress decreases to a steady nonzero value. The first defects

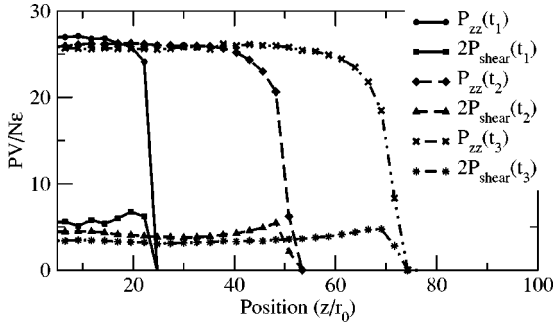

FIG. 1. Uniaxial and shear pressure profiles in reduced units, at three different times. The longitudinal direction is a $\langle 100 \rangle$ direction. The piston velocity is $u_p = 2.3\ \sqrt{\epsilon/m}$.

are detected close to the shock front at time t_1 (Figs. 1 and 2). In the following paragraph, they will be identified as high-pressure Shockley dislocation loops. They are formed homogeneously in a thin slice of about five $\{100\}$ planes moving with the shock front. The MCP shows that the slipped region in the glide plane is a small plate with the shape of an ellipse (Fig. 2). Once initiated, a slipped region expands in all directions in its glide plane, which involves the shearing of the elastically compressed crystal at the back of the nucleation zone, and a propagation of the defect together with the shock front. No ''macroscopic'' shear release is measured on the shear profile in these first moments (Fig. 1). When these defects get wide and dense enough, they intersect and form a cellular mesostructure,[3] which can be associated with a shear stress release (Fig. 1, time t_3).

It happens that the first loop reaches a noticeable size before the smaller ones can intersect it. It is therefore possible to get detailed structural data about a defect subjected only to weaker elastic interactions. Figure 2(a) is a top view of such a loop as revealed by the MCP criterion. The normal to the defect is a $\langle 111 \rangle$ direction (Y axis). X is the direction of easy glide in the fcc structure, namely, $\langle 112 \rangle$ and Z is a $\langle 110 \rangle$ direction [Fig. 2(b)]. The displacement field around the defect is represented by the atom's position on a transverse cut perpendicular to the Z axis (Figs. 2(c) and 2(d)]. Two $\{220\}$ planes are projected on the cut plane (white and black atoms). The elastic uniaxial compression ($\sim 14\%$) has been compensated to highlight the defect position. The horizontal axis is the longitudinal $\langle 100 \rangle$ direction of the crystal, i.e., the compression axis. The stacking fault corresponding to the slipped region is clearly visible. As expected for a shear defect, the plane of the stacking fault is strongly inclined with respect to the compression axis. A close look at the picture will reveal the elastic bending of the planes above and below the stacking fault.

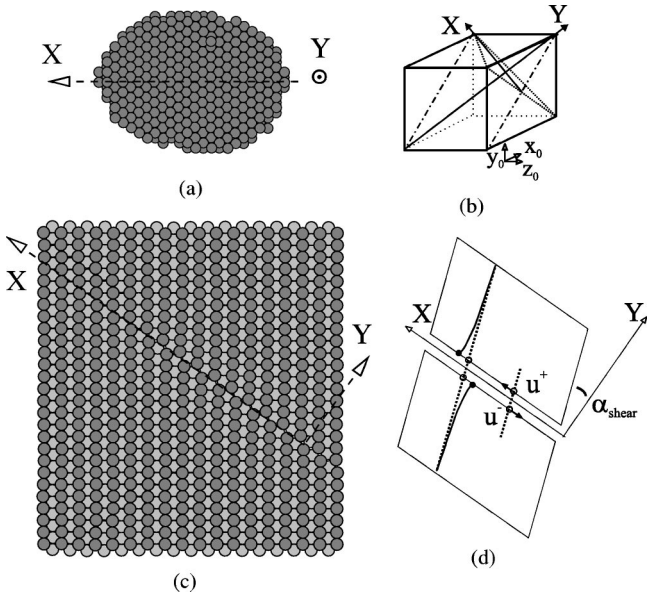

FIG. 2. Detail of a quasi-isolated defect (snapshot). The normal to the slip plane (Y) and the slip direction (X) are presented in (a), where Y and X are, respectively $\langle 111 \rangle$ and $\langle 112 \rangle$ directions. The orientation of (X,Y) with respect to the longitudinal direction Z_0 is shown in (b). Transverse cuts along (X,Y), real (c) and schematic (d), highlight the displacement discontinuity $u^+ - u^-$ across the slip plane. α_{shear} is the resolved shear in the glide direction (X).

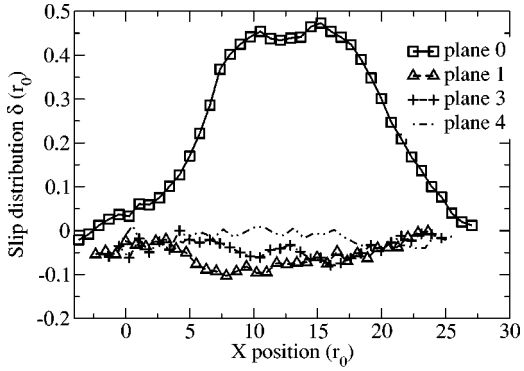

FIG. 3. Slip distribution of the defect represented in Fig. 2. The uniaxial compression is compensated. The reference axes are those of Fig. 2(c).

The essential characteristic of this kind of slip defect is its Burgers vector: the amplitude of slip in the slipped region of the glide plane far from the dislocation line. It can be measured from the slip distribution $(\delta_x^i, \delta_y^i, \delta_z^i)(x)$,

$$\delta_x^i(x) = u_x^{i+1}(x) - u_x^i(x), \tag{2}$$

where u_i is the displacement in the plane i parallel to the glide plane. Figure 3 gives the slip distribution in the X direction corresponding to the configuration of [Fig. 2(c)]. The $\{111\}$ plane immediately below the stacking fault is labeled 0 (i is positive for the planes where $Y \geqslant 0$). The slip distribution shows that, in the inner part of the defect, the slip is $0.45 r_0$ which is the value of the translation used to create a stacking fault ($1/6\langle 112 \rangle$) in the uniaxially compressed crystal (see Sec. IV). The defect is therefore a Shockley partial dislocation loop. The transverse cut in Fig. 2(c), perpendicular to the edge segments, can be viewed as a pair of edge Shockley partial dislocations, of same glide plane, but opposite sign, spontaneously formed in a perfect crystal under high pressure. It is not easy to define the excess planes on this figure because the bending of the planes perpendicular to the glide plane is not localized in the vicinity of the dislocation line. This configuration is the one proposed by Orowan in his early model of local gliding.[9,10] This model gives a

different picture of the displacement of matter after the passage of a dislocation, compared to Polanyi and Taylor lattice dislocation.[10,11] In the first case, the dislocation ''cures'' the shear displacement imposed on the crystal by the external forces. As a consequence, the displacement of the atoms, with respect to the presheared lattice is limited to the vicinity of the glide plane. In Taylor's model, the edge dislocation is represented in an unstrained lattice, and the excess plane can be clearly identified. The defect displacement involves the relative translation of the entire half crystal above and below the slip plane. If the external shear is small, the two models converge. In the simulation, we have confirmed that the displacement of the atoms on two $\{111\}$ planes on each side of the glide plane rapidly converges to a constant value, independent of the atom position with respect to the core of the loop, when the distance between the planes increases. Furthermore, the shear displacement field shows only cooperative translations on the first four planes in the vicinity of the loop. This confirms the adequacy of Orowan's model. The specificity of this high-pressure defect is that its elastic strain field is localized in the *Y* direction and uniformly distributed along the stacking fault, instead of being mainly localized around the dislocation line. It is also clear that there are neither strong interactions between the defects because of displacement field incompatibilities nor between the defects and the shock front or the periodic boundary conditions, at least when the loop radius is small.

FIG. 4. Defect nucleation at $u_p = 2.3\sqrt{\epsilon/m}$. (a) and (b) are tilted around the (010) axis, (b) is a side view of the shock (the propagation occurs towards the right).

III. STUDY OF THE NUCLEATION MECHANISM

We perform MD simulations with piston velocities in the range $[1.9;2.5]$ on shorter but wider samples than before ($90\times90\times76$ $\langle100\rangle$ unit cells). The aim is to localize the defects to gain some statistical information about the nucleation mechanism (nucleation rate, critical defect size, influence of the temperature and of the shear stress).

A. Localization of the nucleation

We use the MCP to detect the formation of defects. A small loop is considered as a nucleus if it contains at least one atom and its first neighbors. Let us recall that the MCP selects the atoms above and below the glide plane, so that an atom in the middle of a stacking fault will have six first neighbors selected in the $\{111\}$ plane where it sits and three in the plane above or below. In this analysis, a defect is therefore a local glide involving at least nine atoms. Figure 4 shows a typical image of an early time of plasticity.

It is clearly visible in Fig. 4 that the small defects (''small'' will be related to a critical size in the following paragraph) are localized in a thin zone of the order of $6r_0$. This is shown quantitatively in Fig. 5, where the loop distribution is represented by two histograms: the number of loops and their average size as a function of the position of their center of mass. The comparison with the shear and temperature profiles shows that loops of under 50 atoms are nucleated just behind the shock front, where the shear and the transverse temperature are maximum. Wider loops obviously have a center of mass further behind the front, but it is worth noticing that their number is small compared to the number of small loops at the front. This is not related to an increase of the nucleation rate in time, but shows that a large fraction of the nuclei at the front do not propagate, but slip back to a perfect lattice configuration. The role of the temperature can be stressed further by noticing that there is not any nucleation at the back of the front, where the temperature profile (Fig. 5) increases with *z*, even if the shear stress is high. Indeed, dislocations are still too few and have not propagated enough to cause a shear release.

Therefore we can spatially decompose the plasticity process: nucleation in a narrow zone behind the shock, where shear and temperature are high, and propagation in the relatively cold but highly sheared region.

B. Critical defect

The nucleation is analyzed within a moving window following the shock front. Only loops of limited size are considered ($\leqslant 700$ atoms). Figure 6 presents the number of loops in this window as a function of time for four different shock strength. For comparison, the maximum transverse temperature is also represented. This value is reached just behind the shock front (Fig. 5).

The onset of plasticity is well correlated with the maximum of the transverse temperature for the various shock strengths. However, the role of temperature is not straightforward: there is no nucleation during the rise time for high shock strength, even if the temperature is higher than what is necessary for nucleation at low shock strength. This indicates

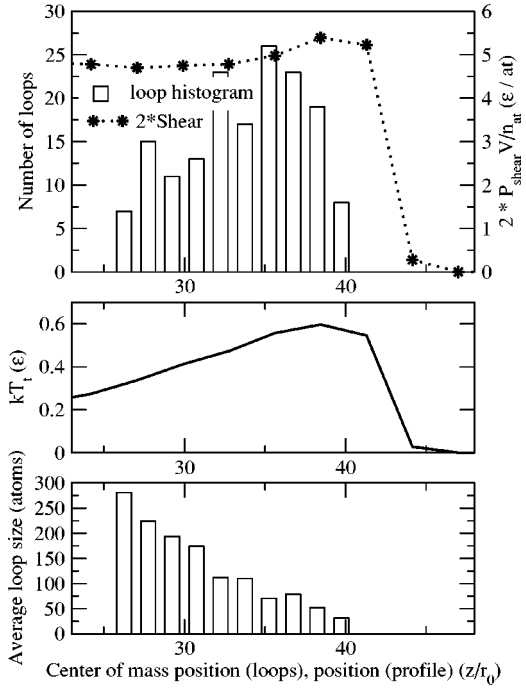

FIG. 5. Localization of the nucleation of the loops. A histogram, representing the number of loops as a function of the position of the loop's center of mass, is superimposed upon the shear pressure profile. The transverse temperature profile and the histogram of the average loop size are presented below. The piston velocity is $u_p = 2.3\sqrt{\epsilon/m}$.

that the creation of nuclei requires the formation of slip fluctuations which are not captured in detail by the transverse temperature.

Since we know (by comparing the number of large loops with the number of nuclei) that a large fraction of nuclei does not propagate, we can look for a critical defect size. For every defect, we measure the size evolution (number of atoms) from the instant when it appears ($t_{nucleation}$). Atoms involved in a local glide are detected every $250\Delta t$. Therefore, the nucleation really takes place between $t_{nucleation} - 250\Delta t$ and $t_{nucleation}$, starting from configurations where only a few atoms are displaced. The critical size is the maximum size a loop can reach before it shrinks and disappears. We distinguish two populations: the undercritical and overcritical defects. The average size of these populations is plotted as a function of time (Fig. 7).

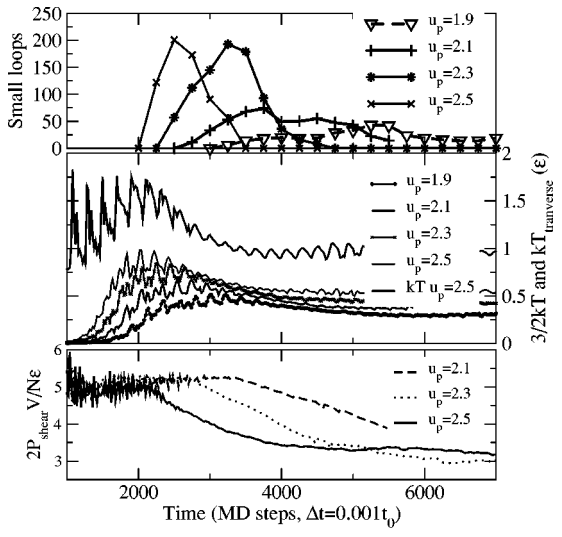

FIG. 6. Time evolution of the number of small loops for u_p between $1.9\sqrt{\epsilon/m}$ and $2.5\sqrt{\epsilon/m}$. The surface section is $90 \times 90\langle 100\rangle$ unit cells.

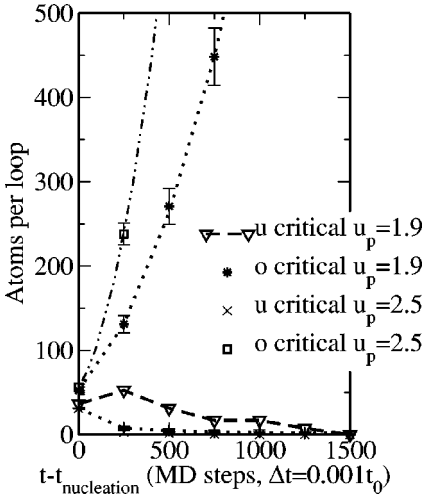

FIG. 7. Time evolution of the number of atoms per loop, averaged over all overcritical loops (stars), large undercritical loops (triangles) for $u_p = 1.9\sqrt{\epsilon/m}$, and under and overcritical loops (crosses and squares) for $u_p = 2.5\sqrt{\epsilon/m}$.

The bars represent the mean-square deviation. For the undercritical population, the bars are small, which reflects that a large number of nuclei can reach 30 atoms in size and then disappear within $500\Delta t$. Nevertheless, by taking the average only over the undercritical loops which have a bit longer lifetime, the curve goes through a maximum close to 50 atoms: the critical size. The piston velocity does not seem to have an influence on the critical defect size, but only on the lifetime of undercritical defects.

C. Dislocation loop propagation

At high piston velocity, the nucleation rate drops as the large loops propagate and release the shear stress (Fig. 7). A possible reason is that the region where the shear stress remains high, behind the shock front, is too narrow for the nuclei to reach the critical size before the shock front moves and the defect sits in the partially relaxed region.

At low piston velocity (1.7 and 1.9) the defect density is low enough to enable the study of the propagation of the large loops (Fig. 8). The velocity of the screw and edge loop segments are measured as a function of the loop diameter. We find that these values rapidly converge to constants. These are 3.2 and 2.4 (LJ units) for edge and screw components, measured by averaging over 40 large loops of the type presented in Fig. 8. This explains why the loops develop in the shape of an ellipse, the long axis being perpendicular to the edge component. The measure is not precise enough to

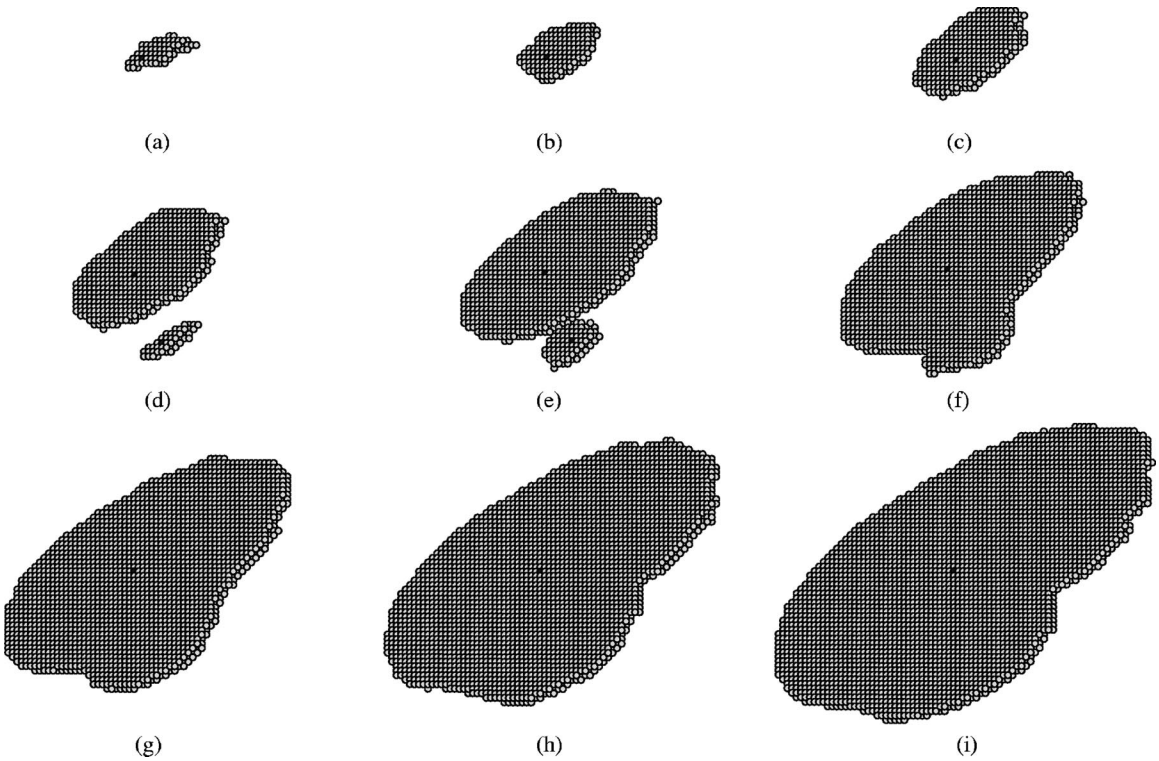

FIG. 8. The pictures, taken every $250\Delta t(\Delta t = 0.001 t_0)$, show the propagation of a loop. (d), (e), and (f): A small defect, lying in the same plane, is absorbed.

see the influence of u_p directly, but it can be estimated from Fig. 7 by assuming that $u_{screw} = 0.8 u_{edge}$, whatever the piston velocity. Then the time evolution of the number of atoms involved in the local glide is a parabolic function of $t - t_{nucleation}$ with the prefactor $0.8 u_{edge}^2$.

Previous studies[4] have shown that, in this crystallographic orientation, the ''plastic wave'' can catch up with the elastic front. We now know that because the nucleation rate is small, the steady plastic wave is caused by the same loops, following the shock front and organized in the mesostructure reported in Ref. 3.

We have shown that plasticity in the $\langle 100 \rangle$ direction is initiated by a nucleation process in a narrow, uniaxially compressed zone, under high temperature, just behind the shock front. We have not discussed the specificity of this crystallographic orientation. In the following section, we compute the activation energy in the Peierls framework and discuss the influence of the $\langle 100 \rangle$ uniaxial compression on the nucleation process.

IV. DRIVING FORCES FOR THE ACTIVATION OF NUCLEATION

As we have detected the nuclei at the back of the shock front in the elastically compressed material, we simplify the problem by considering the homogeneous nucleation in a uniformly deformed crystal. The defects appear, for this crystal orientation, only in a thin slice of matter in the vicinity of the front. There should be an influence of the stress gradient, but we will not consider this in our first approach to the problem.

The nucleation of dislocation loops in perfect crystals has been discussed in the framework of the elastic theory of dislocations.[12] The energy needed to create a loop of radius r has two contributions: the elastic energy stored in the crystal because of the dislocation and the work done by the external shear stress. The shear release obtained by the expansion of the loop $(-\pi r^2 \sigma b)$ compensates the excess elastic energy related to the dislocation line. By optimization of the total energy with respect to the radius of the loop, one obtains the critical radius and the activation barrier that the loop has to overcome. Any smaller defect will shrink back to a perfect crystal. It is shown that the applied shear stress should be close to the theoretical elastic limit ($\mu/30$, far from the domain of validity of linear elasticity) for activating such a mechanism, which is two orders of magnitude higher than the experimental yield point of ductile materials at low deformation rates. In the shock wave simulation, however, the stress levels are high and the classical homogeneous nucleation is likely to be relevant for predicting the onset of plasticity.

One drawback of the elasticity analysis is the core cutoff (several Burgers vectors b) that is used, because this is the order of magnitude of the critical radius we have to deal with. The Peierls-Nabarro concept can be used to overcome this difficulty, as Nabarro did to study the creation of a dislocation dipole[10] and Rice,[13] more recently, to study dislocation emission at a crack tip. This model has been revisited by Bulatov and Kaxiras,[14] who have shown with careful comparison to fully atomistic calculations that it can be used to compute the core structure of dislocations.[15] In this section, we build a semicontinuous model, coherent with the MD

atomistic calculations, and based on the Peierls-Nabarro concept. Following classical nucleation theory, this model is used to compute the critical radius r_c for the creation of Orowan's glide defects, as a function of the predeformation of the crystal, limited for this calculation to a resolved shear in the slip direction. The interest of such a model is the natural separation of the energy between an elastic part coming from the bending of the planes normal to the glide plane [Figs. 2(c) and 2(d)] and the excess energy due to the displacement discontinuity across the glide plane. It highlights the driving forces for the onset of plasticity: the barrier associated with the unstable stacking fault and the elastic energy release distributed all along the stacking fault.

A. Dislocation model

Within the Peierls framework,[16] a dislocation of Burgers vector b is characterized by a distribution of displacement discontinuities $\delta(x)$ across the slip plane [the axes are those of Fig. 2(d)]. To compute the elastic field, without core cutoff, the dislocation is considered to be composed of infinitesimal dislocations. The elementary Burgers vector at position x' is

$$b'(x')dx' = \left(\frac{d\delta}{dx}\right)(x')dx', \tag{3}$$

with

$$\int_{-\infty}^{+\infty} b'(x')dx' = b. \tag{4}$$

The analytical solution from elastic theory for screw and edge dislocations in an unstrained lattice gives the field induced by the elementary dislocation. The stress in the glide plane is obtained by integration over all elementary defects. The stored elastic energy is the work done by the stress on the surfaces of a cut when the dislocation is formed by the Volterra procedure. Bulatov *et al.*[14] developed an energy functional which is composed of this elastic energy, plus a ''core'' energy related to the displacement discontinuity. This last term is estimated by

$$\int \gamma(\delta(x))dS, \tag{5}$$

where γ is the generalized stacking fault energy surface (GSF).[17] The GSF is computed from atomistic models by rigidly translating the crystal above the slip plane with respect to the lower part by a uniform vector δ. Both components, elastic and core energy, are function of $\delta(x)$. By discretizing $\delta(x)$ over the atomic rows, the dislocation structure can be obtained by minimization of the functional with respect to $\{\delta_i\}$.

As a first approach, a shock-induced defect is described by the simplest configuration: an edge dipole which corresponds to the edge segments of the Shockley loop in Fig. 2(c). The energy of this dipole is computed following the energy decomposition exposed above, but without making reference to a distribution of dislocations. We know, from elasticity, that the stress field around a dipole is confined in the vicinity of the defect so that the stored energy does not diverge, contrary to an isolated dislocation. Therefore, we compute the stored elastic energy in a finite rectangular box around the dipole, using finite elements (FE). The defect is no longer viewed as a dipole, but as an Orowan local glide, characterized by a slip distribution $\{\delta_i\}$.

The displacement of the atoms above and below the slip plane, $u^+(x)$ and $u^-(x)$, has to be specified to characterize the slip discontinuity. We chose to use the variable $\delta(x) = u^+(x) - u^-(x)$ instead of $u^-(x)$, because of its relation to the GSF. α_{shear} is the preshear deformation in the glide direction [X, Fig. 2(d)]. Because the $\langle 100 \rangle$ uniaxial compression is contained in the plane composed of the normal to the glide plane and the slip direction (X,Y), there is no deformation out of that plane. Therefore, the problem is two dimensional. The preshear deformation is related to the uniaxial compression in the last paragraph, where the influence of the other components of the resolved deformation are discussed.

The FE mesh is rectangular and related to the atomic scale by the definition of the dimension of the elements ($l_X = \sqrt{3}r_0, l_Y = (\sqrt{6}/3)r_0, l_Z = r_0$), each element containing two atoms. The elastic constants, taken from the atomic potential, are converted from energies per atom (ϵ/at) to energy densities. Since the fcc cell contains four atoms, the conversion implies a factor of $(4/a_0^3)$. With these length and energy scales, the stored elastic energy, obtained by integration over the FE mesh, is consistent with MD. The system is separated into two parts, above and below the glide plane. Border conditions are applied to each part. On the horizontal borders, the displacement is imposed: the displacement due to the preshear on one side (the dimension of the box is large enough to neglect the stress field of the defect on this border) and u^+ or u^- on the other side. On the vertical borders, the stresses imposed to simulate an infinite medium are

$$\sigma = \begin{pmatrix} C_{1112} & C_{1212} \\ C_{1212} & C_{2212} \end{pmatrix} \tan \alpha_{shear}. \tag{6}$$

The system is symmetric with respect to the X axis, so the FE mesh is the same above and below the glide plane; therefore the same rigidity matrix can be used, but with different border conditions.

A configuration is therefore defined by $(\alpha_{shear}, u^+(x), \delta(x), n_c)$, where n_c is the number of $\{111\}$ planes above or below the glide plane that defines the cutoff for the elastic calculation. The total potential energy of the system is the sum of the elastic energy and the core energy (obtained from the GSF). The GSF is computed from the atomistic potential. The fields are discretized by taking their values at the FE nodes. The structure and energy of a loop is obtained by minimization of the numerical functional with respect to u_i^+ and δ_i, some nodes' displacements being constrained to impose the ''radius'' of the slip defect. (α_{shear}, n_c) are parameters.

B. Uniform slip distribution

The excess energies coming from the mixed model and from atomistic calculations are first compared for simple

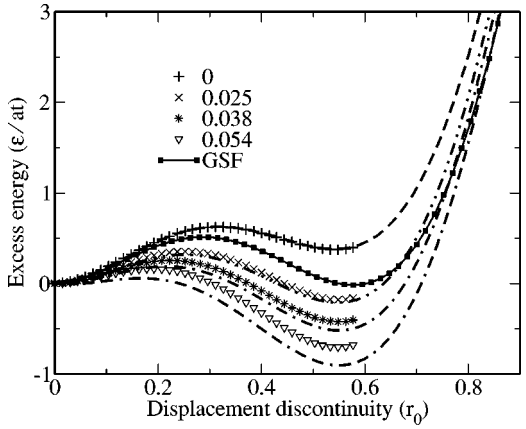

FIG. 9. Excess energy per atom of the stacking fault plane, as a function of the displacement discontinuity δ and for $u^+=0$. The data obtained by MD are represented by symbols, those obtained by the mixed model by lines. The agreement is quantitative for low preshears ($\tan\alpha_{shear}$ is specified in the legend), but only qualitative when $\tan\alpha_{shear}>0.025$.

configurations where u^+ and δ are uniform. In the atomistic calculations, the positions of the atoms of the first planes on each side of the glide plane ($Y=0$) are fixed. The rest of the system, within a cutoff distance is relaxed by quenched molecular dynamics (QMD). A strain field is therefore induced by the energy minimization constrained by the border conditions.

When the defect is infinite, the cutoff has an important influence on the value of the stored energy. Let us consider that the elastic field is the uniform shear: $\tan\alpha_{shear}=1/n_c$. So, if n_c becomes large, the shear goes to zero, and the configuration is the same as two half crystals translated, respectively, by $\delta=1$: the stored elastic energy decreases to zero and the excess energy reduces to the GSF. The cutoff has no real meaning here, but we set it arbitrarily to 20 $\{111\}$ planes, in order to have a nonzero stored elastic energy, thereby enabling the discussion of the shear release.

The excess energy $E(\delta)$, for $u^+=0$ and $n_c=20$, as a function of the preshear ($\tan\alpha_{shear}$) are presented in Fig. 9. The QMD (symbols) and mixed calculation (lines) are in excellent agreement for $\alpha_{shear}=0$. The comparison with the GSF shows how the elastic distortions add up to the slip discontinuity to increase the energy barrier for slip nucleation.

When the crystal is prestrained, the comparison between the two models is still quantitative up to $\tan\alpha_{shear}=0.02$ (Fig. 9) and only qualitative above. At $\tan\alpha_{shear}=0.054$, which is close to the resolved shear at the MD elastic limit, we have checked that the difference is of the order of 30%. The elastic relaxation of the shear stress is overestimated. As a consequence, the elastic limit obtained by the mixed model should be too low. One reason for this is probably that the prestraining is outside the range of validity of linear elasticity. The calculation of the energy of a sheared perfect crystal from atomistics already shows a discrepancy of the order of 30% with linear elasticity. Including higher-order terms would probably improve the model, but it is out of the scope of this work, which is dedicated to the qualitative discussion of the driving forces for defect nucleation under high pressure.

One of the driving forces is the shear release. In the case of uniform $\{\delta_i\}$, the mixed model shows that the elastic bending of the planes normal to the glide plane relaxes the preshear, contrary to the case at zero prestrain. Not only is the energy at the unstable stacking fault (USF) position lowered, but also the stacking fault energy (SFE) at the intrinsic position is lowered. This means that the energy barrier is lowered and that an infinite stacking fault is stabilized. This is particularly striking here because the SFE is already low in an unstressed crystal (a drawback of the LJ pair potential), but this analysis shows that even in the case of a positive SFE, the crystal could develop local glide defects, provided that the defect and the preshear are large enough to induce a noticeable shear release.

A finite-size glide defect would have a δ-distribution spread over the entire spectrum. The inner part of a large loop will fall in the range where the SFE is compensated by the shear release. Therefore the negative excess energy of the inner part of the defect can compensate the high energy of the dislocation line: the border between the slipped and the unslipped portion of the glide plane, where most of the atoms fall in the region which corresponds to the USF. This is, qualitatively, the origin of the critical radius which is computed below.

C. Local glide defect excess energy at high pressure

The configuration considered here is an edge dipole under high pressure. The critical separation of the dipole is computed using the mixed model, for preshears ranging from $\tan\alpha_{shear}=0.02$–0.055. We know from the uniform slip distribution analysis that, above $\tan\alpha_{shear}=0.02$, there are values of u^+ and δ which involve an energy decrease. Therefore, it is possible to find the structure of a finite (eventually large) defect for shears higher than this value. The procedure is the following.

(1) The initial configuration characterizes the width of the defect: the inner dipole nodes are those where u^+ and δ are set to nonzero values and are not constrained. All other nodes in the glide plane (outer dipole nodes) have fixed, zero, u^+ and δ values.

(2) The energy is minimized with respect to u^+ and δ of the inner dipole nodes.

(3) If a metastable configuration comes out of the minimization, the defect width and the excess energy per inner loop atom are measured. If the configuration goes to zero, whatever the initial values of u^+ and δ, the width that we try to impose is below the dipole critical separation r_c.

The definition of a cutoff radius is critical for the elasticity calculation because the excess elastic energy is an integral over a large region. A cutoff that is too short can lead to large errors (100%). It was defined here by taking a configuration and computing the energy as a function of the number nodes in the direction normal to the glide plane *N*. The calculations show that the excess energy converges for *N* equal to twice the number of inner loop nodes, which means that

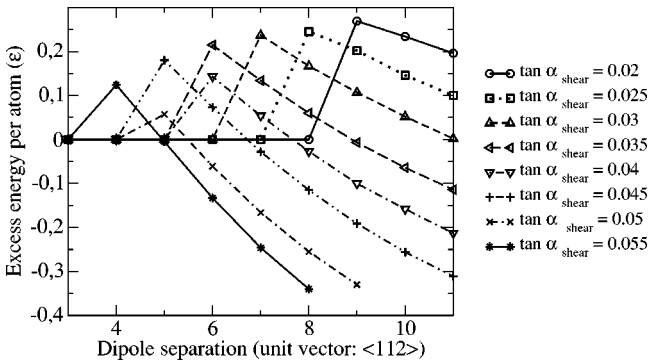

FIG. 10. Excess energy per atom of the dipole configuration, as a function of the separation between the dislocations.

the stress field is negligible at distances higher than the dipole separation ($l_y \approx 0.47 l_x$), in agreement with dislocation elasticity theory. We expect similar results in the case of 3D loops. It gives some confidence that the periodic boundary conditions should only have a limited influence on the nucleation and the first moments of propagation of the loops in the NEMD simulations, as checked in Ref. 3. As long as their radius is noticeably smaller than the transverse dimensions of the box, they do not interact with themselves.

The maximum excess energy at fixed α_{shear} found in this calculation is taken as the activation energy (E_a) (Fig. 10). The mixed model shows that E_a (respectively r_c) decreases linearly as a function of $\tan\alpha_{shear}$ from $0.25\epsilon/at$ (respectively $9\sqrt{6}r_0$) at $\tan\alpha_{shear}=0.02$ to $0.12\epsilon/at$ at $\tan\alpha_{shear}=0.055$ (respectively $4\sqrt{6}r_0$). By extrapolation, we find that E_a is of the order of $0.1\epsilon/at$ for small defects ($r_c \approx 3\sqrt{6}r_0$). For a $\langle 100\rangle$ uniaxial compression the resolved shear $\tan\alpha_{shear}$ is related to the compression λ by

$$\tan\alpha_{shear}=\frac{\sqrt{2}}{9}\,\frac{(1+2\lambda)(\lambda-1)}{\lambda}, \tag{7}$$

which gives $\lambda \approx 0.85$ for $\tan\alpha_{shear}\approx 0.064$. This is the elastic limit given by the NEMD simulations. We give a qualitative estimate of the activation energy in 3D by considering that the critical loop observed in MD involves 25 atoms, each carrying an E_a of $0.1\epsilon/at$. The energy barrier is therefore 2.5ϵ, of the same order of magnitude of the temperature behind the shock ($3kT/2 \approx 2\epsilon$).

The mixed model gives a good order-of-magnitude estimate for the excess energies compared to the NEMD simulations. It enables a qualitative discussion of the importance of the GSF versus elastic distortions in the excess energy of the loops. The energy decomposition shows that the elastic energy is not negative for the tiny loops, as opposed to the large loops. For these configurations, the δ distribution is very steep with a plateau value ($0.4r_0$) intermediate between the unstable and the intrinsic stacking fault. Therefore, the metastable configuration stems from a balance between the tendency to place the inner atoms as close as possible to the intrinsic stacking fault configuration and the elastic distortions that it involves at the dislocation line.

For the Lennard-Jones potential, the GSF is only weakly modified by the preshear, but more largely by the uniaxial

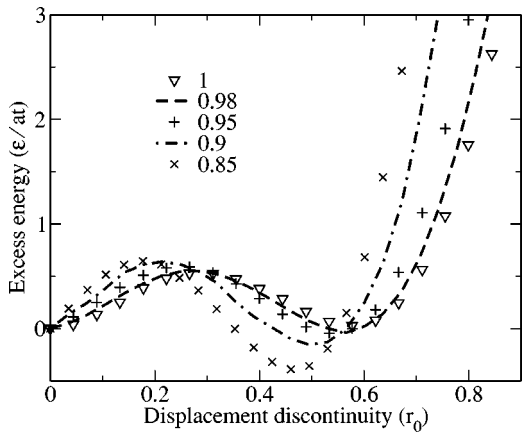

FIG. 11. Influence of a uniaxial compression in the $\langle 100\rangle$ direction on the γ surface.

$\langle 100\rangle$ compression (Fig. 11). γ_{us} is not affected, whereas the γ_{sf} is largely negative, which is in favor of the formation of tiny loops. On the contrary, in the on-top position, the excess energy is increased by a factor 2. This has no effect here, because this part of the GSF is never explored during the slip process. Nevertheless, it is an indication that the predeformation might increase γ_{us} and γ_{sf} if, contrary to the $\langle 100\rangle$ compression, the deformation out of the plane composed by the glide direction and the normal to the slip plane (OX, OY in Fig. 2) is not zero. This could increase the elastic limit even in shock directions vicinal to $\langle 100\rangle$.

The tendency of having a negative intrinsic stacking fault energy with increasing compression is a well-known drawback of the Lennard-Jones potential. Even if we have shown the important role played by γ_{us} and γ_{sf}, it is a nontrivial task to try to reproduce these quantities with an *n*-body potential (such as embedded atom method) for a specific metal. Not only it requires *ab initio* data under uniaxial compression, but it has been shown recently that γ_{sf} under compression depends on long-range interactions.[18]

V. CONCLUSION

We have studied the plasticity mechanism in a perfect, infinite, $\langle 100\rangle$ single crystal submitted to a moderate shock. A picture of the nucleation process, at the atomic scale, is obtained by NEMD simulations. They show that the shear stress is partially released on the picosecond time scale by the formation of Orowan's local glide defects: a high-pressure version of a dislocation loop with Burgers vector $\frac{1}{6}\langle 112\rangle$. These loops are created by thermal fluctuations in a narrow region of five lattice parameters width, just behind the front. In these early moments, the shear stress is high and the whole sample behind the shock is uniaxially compressed. However, there is no nucleation until the transverse temperature reaches its peak value, highlighting an activated process. A careful investigation of the time evolution of the defect population gives evidence of a critical size, at an atomic level, above which a loop expands with no possibility to slip back to a perfect configuration. Such defect is a 5×5 atom^2 area of local glide.

The activation energy is estimated by a semiquantitative calculation of the formation energy of an edge dipole in the Peierls framework. The calculation shows a linear decrease of E_a with the resolved shear in the slip direction. By extrapolation, we find an activation energy of 2.5ϵ for the critical defect, a value of the same order of magnitude as the temperature ($3kT/2 \approx 2\epsilon$) in the nucleation zone. The use of the Peierls model has shown that shear relaxation is the driving force for the propagation of large loops, but not for the formation of tiny loops. In this case, elastic distortions at the dislocation line add up to the GSF. We have shown that both the unstable and intrinsic stacking fault energies under high pressure play an essential role in the formation of the critical defect.

Further work should incorporate initial defects such as grain boundaries or impurity clusters and study the effects of stress concentration on plastic flow initiation. This would be an intermediate step between the perfect single crystals and the real systems where the initial microstructure probably plays a crucial role.[19] In single crystals, further work should focus on a quantitative calculation of the activation energy or critical stress for vicinal orientations, in order to test the orientation dependence of the elastic limit. In particular, the energy saddle points corresponding to the tiny defects should be investigated by a more accurate method. Furthermore, previous work[4] has shown different plasticity mechanisms for $\langle 111 \rangle$ and $\langle 110 \rangle$ orientations, which still lack structural explanations.[20]

ACKNOWLEDGMENTS

We wish to acknowledge Robb Thompson, Kai Kadau, and Jim Hammerberg (Los Alamos Nat. Lab.). D.T. also thanks Professor R. Fortunier (Ecole des Mines de Saint-Etienne) for his support for the elastic calculations.

*Electronic address: tanguy@emse.fr

[1] C.S. Smith, Trans. Metall. Soc. AIME **212**, 574 (1958).
[2] B.L. Holian, Shock Waves **5**, 149 (1995).
[3] B.L. Holian and P.S. Lomdahl, Science **280**, 2085 (1998).
[4] T.C. Germann, B.L. Holian, P.S. Lomdahl, and R. Ravelo, Phys. Rev. Lett. **84**, 5351 (2000).
[5] D.M. Beazley and P.S. Lomdahl, Comput. Phys. **11**, 230 (1997).
[6] D.J. Honeycutt and H.C. Andersen, J. Phys. Chem. **91**, 4950 (1987).
[7] A. Aslanides and V. Pontikis, Philos. Mag. A **80**, 2337 (2000).
[8] C.L. Kelchner, S. Plimpton, and J.C. Hamilton, Phys. Rev. B **58**, 11 085 (1998).
[9] E. Orowan, Z. Phys. **89**, 634 (1934).
[10] F.R.N. Nabarro, *Theory of Crystal Dislocations* (Dover, New York, 1987).
[11] M. Polanyi, Z. Phys. **89**, 660 (1934).
[12] A.H. Cottrell, *Dislocations and Plastic Flow in Crystals* (Oxford University Press, London, 1953).
[13] J.R. Rice, J. Mech. Phys. Solids **40**, 239 (1992).
[14] V.V. Bulatov and E. Kaxiras, Phys. Rev. Lett. **78**, 4221 (1997).
[15] G. Lu, N. Kioussis, V.V. Bulatov, and E. Kaxiras, Phys. Rev. B **62**, 3099 (2000).
[16] J. P. Hirth and J. Lothe, *Theory of Dislocations* (Wiley, New York, 1982).
[17] V. Vitek, Philos. Mag. **18**, 773 (1968).
[18] G.S. Fanourgakis, V. Pontikis, and G. Zérah, Phys. Rev. B **67**, 094102 (2003).
[19] J. Sharma, in Proceedings of TMS Meeting, San Diego, 2003 (unpublished).
[20] R. Ravelo, T. C. Germann, D. Tanguy, M. Mareschal, P. S. Lomdahl, and B. L. Holian (unpublished).